STU
FCHPT

Reaction mode of catalytic styrene oxidation using a bis-semicarbazide hexaazamacrocyclic Cu complex

Martin Breza

Department of Physical Chemistry, Faculty of Chemical and Food Technology STU, Radlinskeho 9, SK-81237 Bratislava, Slovakia
martin.breza@stuba.sk

Abstract: Catalytic styrene Ph—CH═CH_2 oxidation is assumed to be a simple reaction procedure; however, its details require further systematic research. Using quantum-chemical treatment, relevant intermediates have been investigated in various charge and spin states of alternative reaction pathways of styrene oxidation by hydroperoxyl using the $[CuL]^-$ catalyst, where H_2L = *trans*-2,9-dibutyl-7,14-dimethyl-5,12-di(4-methoxyphenyl)-1,2,4,8,9,11-hexaazacyclotetradeca-7,14-diene-3,10-dione. Within reaction pathway A, the neutral hydroperoxyl radical is bonded to Cu to form $^2[CuL(OOH)]^-$. Subsequent addition of neutral styrene results in the formation of $^2\{[CuL(OH)](Ph—CH_2—CHO)\}^-$. Reaction pathway B starts with the initial non-radical formation of the π-complex $^1[CuL(Ph—CH═CH_2)]^-$ which is problematic due to its endothermic character. Subsequent addition of a hydroperoxyl radical leads to $^2\{CuL[Ph—CH(OOH)—CH_2]\}^-$ and its oxidation leads to the separation of Ph—CH(OOH)—CH_2. The exothermic reaction path A is preferred over the endothermic reaction path B.

Keywords: B3LYP hybrid functional; broken symmetry treatment; Cu oxidation state; electronic structure; geometry optimization

Introduction

Catalytic oxidation of styrene is an environmentally friendly path of benzaldehyde production, which is an important intermediate in the production of many fine compounds and commodity chemicals (Andrade et al., 2021). Various catalysts differ in the conversion and selectivity of benzaldehyde, styrene epoxide, phenylacetaldehyde, 1-phenylethane-1,2-diol, benzoic acid, phenylacetaldehyde, and other oxidation products. The development of sustainable and effective catalytic systems for benzaldehyde production using green oxidants, such as hydrogen peroxide, is highly significant. For rational design of efficient catalysts, the corresponding reaction mechanisms must be known. Redox-active ligands can contribute by storing and providing electrons, modifying the Lewis acidity of the metal and assisting the formation/breaking of substrate bonding.

Catalytic styrene oxidation is assumed to be a simple reaction procedure, but its details require further systematic research as they are crucial for the development of new catalytic systems. Despite intense studies on the catalyzed oxidation of alkenes with hydrogen peroxide, no generally accepted mechanism of these reactions is known.

The Wacker process (Keith and Henry, 2009) is industrial homogeneous catalytic oxidation of ethylene to acetaldehyde in the presence of $PdCl_2$ and $CuCl_2$ and it is considered to be well understood. Its mechanism is based on active intermediate $[PdCl_2(C_2H_4)(H_2O)]$ with ethylene π-bonded to Pd(II) central atom.

However, other catalytic studies using the 1st row transition metal complexes with multidentate ligands suppose that intermediate M—O—O—H (M is the metal center) is formed and the O—O bond is activated to enable the alkene's reaction (Zhou et al., 2010; Lashanizadegan et al., 2017; Lashanizadegan et al., 2021; Lashanizadegan et al., 2022; Yang and Sarazen, 2022; Wu et al., 2023; Abuhafez et al., 2024; Vala et al., 2024; Razmara et al., 2025; Saveh et al., 2025). Most of these studies are restricted to quantum-chemical modeling of the catalyst (Lashanizadegan et al., 2017; Lashanizadegan et al., 2021; Lashanizadegan et al., 2022; Yang and Sarazen, 2022; Vala et al., 2024; Razmara et al., 2025; Saveh et al., 2025) or its complex with hydroperoxyl (Yang and Sarazen, 2022). The reaction pathway for styrene epoxidation with H_2O_2 using the 8-hydroxylquinolinmanganese(III) complex $[Mn^{III}Q_2Cl]$ in water was modeled as follows (Zhou et al., 2010):

$$[Mn^{III}Q_2Cl] + HOOH \rightarrow [Mn^{III}Q_2Cl(HOOH)] \quad (1)$$

$$[Mn^{III}Q_2Cl(HOOH)] \rightarrow [Mn^{IV}Q_2Cl(OH)]^+ + OH^- \quad (2)$$

$$[Mn^{III}Q_2Cl(HOOH)] + Ph—CH═CH_2 \rightarrow \rightarrow Ph—CHOCH_2 + [Mn^{III}Q_2Cl] + OH^- + H^+ \quad (3)$$

$$[Mn^{IV}Q_2Cl(OH)]^+ + Ph—CH═CH_2 \rightarrow \rightarrow Ph—CHOCH_2 + [Mn^{III}Q_2Cl] + H^+ \quad (4)$$

Another reaction pathway for the oxidation of sty-

rene with O_2 using a cobalt(III)-tetraphenyl catalyst [$HCo^{III}(TPP)$] was modeled without any solvent as follows (Abuhafez et al., 2024):

$$[HCo^{III}(TPP)] + Ph—CH{=}CH_2 \rightarrow \rightarrow [Co^{II}(TPP)]^{\bullet} + (Ph—CH—CH_3)^{\bullet} \quad (5)$$

$$[Co^{II}(TPP)]^{\bullet} + (Ph—CH—CH_3)^{\bullet} + O_2 \rightarrow \rightarrow [Co^{III}(TPP)—O—O—CHPh—CH_3] \quad (6)$$

$$[Co^{III}(TPP)—O—O—CHPh—CH_3] \rightarrow \rightarrow [Co^{III}(OH)(TPP)] + Ph—CO—CH_3 \quad (7)$$

Subsequently, the catalyst was regenerated using Et_3SiH.

In our previous study (Dobrov et al., 2020), the CuL complex (Fig. 1) with *trans*-2,9-dibutyl-7,14-dimethyl-5,12-di(4-methoxyphenyl)-1,2,4,8,9,11-hexaazacyclotetradeca-7,14-diene-3,10-dione (H_2L), a 14-membered bis-semicarbazide hexaazamacrocycle, was synthesized and characterized by analytical and spectroscopic techniques (IR, UV–vis, ^1H and ^{13}C NMR, ESI mass spectrometry, single-crystal X-ray diffraction, and spectroelectrochemistry). This complex selectively catalyzes microwave-assisted oxidation of neat styrene to benzaldehyde using hydrogen peroxide (30 % aqueous solution) as the oxidizing agent under low microwave irradiation (25 W) and in the absence of any added solvent. Under optimized conditions (40 min of irradiation at 80 °C), the catalytic system provided benzaldehyde yields of up to 81 % (turnover frequency up to 2.4×10^3 h^{-1}) as the only product. The CuL catalyst can be very simply separated by cooling to room temperature.

In Dobrov et al. (2020), a free radical mechanism for catalytic oxidation of styrene was proposed initiated by Cu-assisted formation of hydroxyl or hydroperoxyl radicals.

Now, two alternative mechanisms of styrene oxidation by hydrogen peroxide using CuL catalysis are investigated by quantum-chemical treatment. Our study is restricted to the structure, energy, and electron structure of relevant intermediates within these reaction pathways:

i) Reaction pathway A starts with the formation of $[CuL(OOH)]^q$ complex followed by styrene addition.
ii) Reaction pathway B starts with the formation of π-complex $[CuL(Ph—CH{=}CH_2)]^q$ and subsequent addition of hydroperoxyl.

The reaction pathways in literature (Zhou et al., 2010; Abuhafez et al., 2024) are related to changes in the oxidation states of the transition metal atom (Mn(III)/Mn(IV), Co(III)/Co(II), see Eqs. (1)–(7)) and the spin states of reaction intermediates are not considered. Therefore, in our reaction model systems, all intermediates are studied in various charge q and spin states to account for the non-innocent character of ligand L^{2-} and possible Cu(II)/Cu(I) equilibria. DFT calculations in Dobrov et al. (2020) are restricted to the CuL complex in various oxidation and spin states only. Possible reaction paths of catalytic styrene oxidation were not investigated by means of theoretical chemistry. In our recent study, this omission is addressed. The main aim of our preliminary DFT study was to propose which of the catalytic reaction pathways (A or B) is more probable and to identify the charge and spin states of their relevant reaction intermediates. Obtained results should enable proposing a realistic reaction pathway, which can be later studied in more detail.

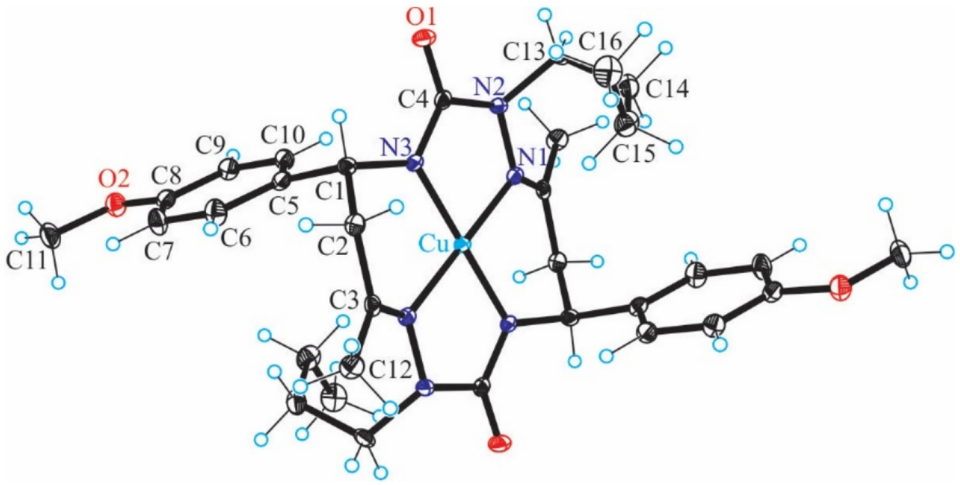

Fig. 1. X-ray structure of CuL with atom-labeling scheme and thermal ellipsoids drawn at 50 % probability level (Dobrov et al., 2020).

Methods

Geometry optimization of the systems under study was performed using B3LYP hybrid functional (Becke, 1993) and 6-311+G* basis sets from the Gaussian library (Frisch et al., 2016) in analogy with our previous study (Dobrov et al., 2020). Optimized structures were tested for the absence of imaginary vibrations using vibrational analysis. Singlet spin states in Cu complexes were treated using unrestricted formalism and their energies related to triplet spin states were corrected as follows ('broken symmetry' treatment, BS) (Malrieu and Trinquier, 2012)

$$E_S - E_T = \frac{\left\langle S^2 \right\rangle_T (E_{BS} - E_T)}{\left\langle S^2 \right\rangle_T - \left\langle S^2 \right\rangle_{BS}} \quad (8)$$

where E_S, E_T, and E_{BS} are singlet, triplet, and 'broken symmetry' (unrestricted singlet) energies, respectively. $\langle S^2 \rangle_T$ and $\langle S^2 \rangle_{BS}$ are triplet and 'broken symmetry' values of spin squares, respectively. Atomic charges, spin populations, and overlap weighted bond orders were evaluated in terms of natural population analysis (Foster and Weinhold, 1980; Reed et al., 1988; Carpenter and Weinhold, 1988). All quantum-chemical calculations were performed using the Gaussian16 software (Frisch et al., 2016). The MOLDRAW software was used for geometry manipulation and visualization (Ugliengo, 2012).

Results

Reaction pathway A

Energy parameters of DFT optimized styrene, hydroperoxyl, $[CuL]^q$ and relevant reaction intermediates in various charge and spin states are presented in Tabs. 1 and A1–A3 of Appendix.

Geometry of $[CuL]^q$ was optimized starting from its X-ray structure (Dobrov et al., 2020) as well as with added hydroperoxyl (starting from the Cu—O distance of ca 2.2 Å) in various charge and spin states (spin multiplicity is denoted as the left superscript where necessary). After geometry optimization, the original square-planar $[CuL]^q$ complex changed its coordination to square-pyramidal only in case of anionic doublet $^2[CuL(OOH)]^-$ (Tabs. A2 and A3 in Appendix, Figs. 2–3, and A1–A2 in Appendix) while its neutral analogues contain the neutral hydroperoxyl radical $(O—O_H—H_O)^0$ (see atomic charges in Tab. 2, spin populations in Tab. 3, and bond orders in Tab. 4) attached by hydrogen bonding $H_O \cdots N3$ (N3 has the highest negative charge and spin population among nitrogen atoms, see Tabs. 2 and 3) without any Cu—O bonds (see Tab. 4, Fig. A2, and Tabs. A2–A3 in Appendix).

Anionic complexes $^1[CuL]^-$ and $^2[CuL(OOH)]^-$ are more stable than their neutral analogues (Tabs. 1 and A1 in Appendix). It can be deduced that they are related by the following exothermic reaction

$$^1[CuL]^- + {}^2(OOH)^0 \rightarrow {}^2[CuL(OOH)]^- \quad (9)$$

as indicated by the reaction Gibbs energy, $\Delta_r G_{298}$ = –56.37 kJ/mol under normal conditions (Tab. A1 in Appendix).

Spin population in $^2[CuL(OOH)]^-$ is located mainly at Cu, unlike the spinless $^1[CuL]^-$ anion. Consequently, spin transfer from neutral hydroperoxyl radical to central Cu atom can be concluded in reaction (9) connected with weakening of the $O—O_H$ bond (Tabs. 3 and 4).

Subsequent addition of neutral styrene to the hydroperoxyl group in $^2[CuL(OOH)]^-$ (due to sterical reasons, C_β must be close to O, and C_α close to OH) causes hydrogen and oxygen transfers resulting in $^2\{[CuL(OH)](Ph—CH_2—CHO)\}^-$ where $Ph—CH_2—CH═O$ is only weakly bonded to $[CuL(OH)]^-$ (Fig. 4, Tabs. 4 and A2–A3 in Appendix). Here, the O atom originally bonded to Cu is shifted to C_β simultaneously with H transfer from C_β to C_α and Cu is bonded to O_H of hydroperoxyl. It is interesting that a removal of one electron results in analogous neutral complexes (Fig. A3, Tabs. A2–A3 in Appendix) with significantly higher energies (Tabs. 1 and A1 in Appendix). Consequently, $C_\alpha—C_\beta$ bonds are weakened and double $C_\beta═O$ bonds are formed (Tab. 4). The strength of Cu—O bond is comparable with that of Cu—N1/N3 (Tab. 4) and the Cu coordination is square-pyramidal (unlike the square-planar $[CuL]^q$, see Tabs. A2–A3 in Appendix). Non-vanishing spin populations in compounds within this reaction pathway can be at Cu, N1, N3 and hydro(pero)xyl oxygen atoms (Tab. 3). Cu in $^1[CuL]^-$ has a less positive charge and no spin population, which implies the oxidation state of Cu(I) (Tab. 2). More positive Cu charges and nonzero spin populations in other compounds of this reaction pathway correspond to the oxidation state Cu(II).

The most probable styrene oxidation step can be described by the exothermic reaction

$$^2[CuL(OOH)]^- + Ph—CH═CH_2 \rightarrow \\ \rightarrow {}^2\{[CuL(OH)](Ph—CH_2—CHO)\}^- \quad (10)$$

as indicated by the reaction Gibbs energy, $\Delta_r G_{298}$ = –266.67 kJ/mol under normal conditions (Tab. A1 in Appendix).

Tab. 1. Relative DFT energies, ΔE_{DFT}, and Gibbs energies at 298 K, ΔG_{298}, of compounds under study with charges q and spin multiplicities M_s. Energy values are related to the most stable systems (in bold) of the same composition.

	q	M_s	ΔE_{DFT} [kJ/mol]	ΔG_{298} [kJ/mol]
$(OOH)^q$	0	2	94.99	97.20
	–1	**1**	**0.00**	**0.00**
	–1	3	67.03	53.90
Reaction path A				
$[CuL]^q$	0	2	127.26	148.50
	–1	**1**	**0.00**	**0.00**
	–1	3	90.95	97.98
	+1	1	748.24	776.49
	+1	3	778.22	799.62
$[CuL(OOH)]^q$	0	1	224.48	232.30
	0	3	224.43	226.92
	–1	**2**	**0.00**	**0.00**
$\{[CuL(OH)](Ph—CH_2—CHO)\}^q$	0	1	322.18	341.47
	0	3	323.41	333.39
	–1	**2**	**0.00**	**0.00**
Reaction path B				
$[CuL(Ph—CH=CH_2)]^q$	**–1**	**1**	**0.00**	**0.00**
	–1	3	37.81	20.01
	0	2	85.46	74.80
$\{CuL[Ph—CH(OOH)—CH_2]\}^q$	0	1	184.97	182.87
	0	3	197.46	188.30
	–1	**2**	**0.00**	**0.00**

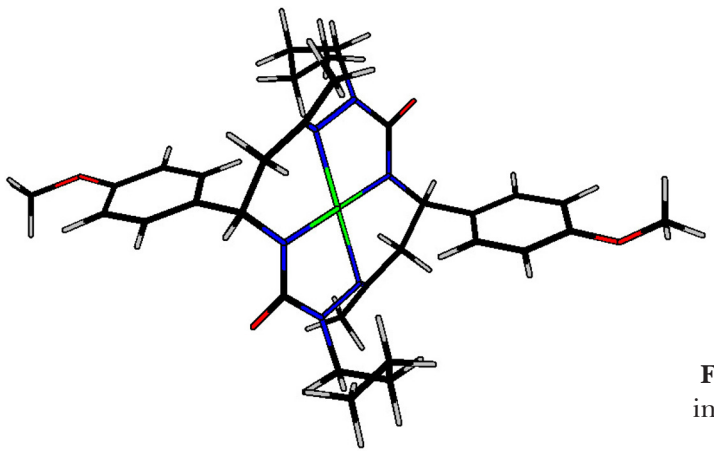

Fig. 2. DFT optimized structure of $[CuL]^-$ in singlet spin state (Cu — green, C — black, N — blue, O — red, H — gray).

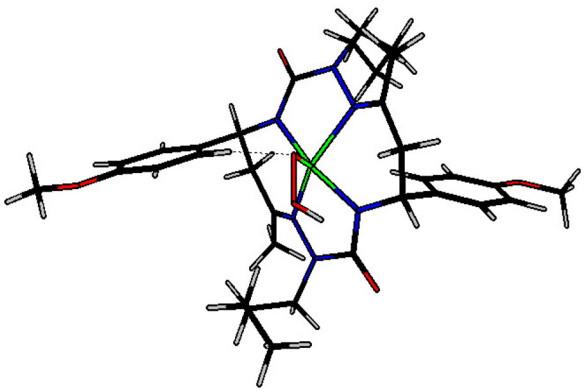

Fig. 3. DFT optimized structure of $[CuL(O—O_H—H_O)]^-$ in doublet spin state (Cu — green, C — black, N — blue, O — red, H — gray).

Tab. 2. Natural charges of C_α, C_β, O, O_H, and H_O atoms in (O—O_H—H_O) and (Ph—C_αH═$C_\beta H_2$) units, and Cu and N atoms in the complexes under study with charges q and spin multiplicities M_s. Data related to systems included in reaction paths A and B are in bold.

	q	M_s	C_α	C_β	O	O_H	H_O
$(OOH)^q$	**0**	**2**	**–**	**–**	**–0.145**	**–0.305**	**0.450**
	–1	1	–	–	–0.767	–0.630	0.396
	–1	3	–	–	–0.511	–0.890	0.401
Ph—CH═CH_2	**0**	**1**	**–0.191**	**–0.346**	**–**	**–**	**–**
Reaction path A							
$[CuL(OOH)]^q$	0	1	–	–	–0.167	–0.317	0.484
	0	3	–	–	–0.167	–0.317	0.484
	–1	**2**	**–**	**–**	**–0.614**	**–0.514**	**0.437**
$\{[CuL(OH)](Ph—CH_2—CHO)\}^q$	0	1	–0.488	0.446	–0.566	–0.925	0.433
	0	3	–0.488	0.448	–0.561	–0.856	0.437
	–1	**2**	**–0.491**	**0.436**	**–0.584**	**–1.188**	**0.424**
Reaction path B							
$[CuL(Ph—CH═CH_2)]^q$	**–1**	**1**	**–0.277**	**–0.472**	**–**	**–**	**–**
	–1	3	–0.240	–0.452	–	–	–
	0	2	–0.192	–0.356	–	–	–
$\{CuL[Ph—CH(OOH)—CH_2]\}^q$	0	1	0.019	–0.251	–0.327	–0.452	0.461
	0	3	0.012	–0.228	–0.319	–0.452	0.457
	–1	**2**	**0.081**	**–0.785**	**–0.347**	**–0.454**	**0.440**
H_2L	0	1	–	–0.357(2×)		–0.680(2×)	–0.383(2×)
Reaction path A							
$[CuL]^q$	0	2	0.927	–0.339(2×)		–0.787(2×)	–0.363(2×)
	–1	**1**	**0.603**	**–0.356(2×)**		**–0.784(2×)**	**–0.404(2×)**
	–1	3	0.853	–0.334		–0.748	–0.373
				–0.504		–0.781	–0.366
$[CuL(OOH)]^q$	0	1	0.925	–0.348(2×)		–0.859	–0.350
						–0.793	–0.355
	0	3	0.925	–0.348(2×)		–0.859	–0.350
						–0.793	–0.355
	–1	**2**	**0.903**	**–0.315**		**–0.777**	**–0.369(2×)**
				–0.332		**–0.750**	
$\{[CuL(OH)](Ph—CH_2—CHO)\}^q$	0	1	0.923	–0.296		–0.651	–0.350
				–0.303		–0.677	–0.347
	0	3	0.955	–0.295		–0.670	–0.337
				–0.307		–0.722	–0.348
	–1	**2**	**0.956**	**–0.312**		**–0.751**	**–0.376**
				–0.317		**–0.743**	**–0.356**
Reaction path B							
$[CuL(Ph—CH═CH_2)]^q$	**–1**	**1**	**0.670**	**–0.326**		**–0.785**	**–0.411**
				–0.270		**–0.782**	**–0.356**
	–1	3	0.885	–0.377		–0.774	–0.372(2×)
				–0.396		–0.781	
	0	2	0.928	–0.340		–0.787	–0.362(2×)
				–0.342		–0.783	
$\{CuL[Ph—CH(OOH)—CH_2]\}^q$	0	1	0.931	–0.340		–0.787	–0.363
				–0.342		–0.784	–0.363
	0	3	0.926	–0.341		–0.787	–0.362
				–0.341		–0.780	–0.363
	–1	**2**	**0.848**	**–0.310(2×)**		**–0.778**	**–0.390**
						–0.759	**–0.351**

Tab. 3. Natural spin populations at C_α, C_β, O, O_H, and H_O atoms in (O—O_H—H_O) and (Ph—C_αH=$C_\beta H_2$) units, and Cu and N atoms in the complexes under study with charges q and spin multiplicities M_s. Data related to systems included in reaction paths A and B are in bold.

	q	M_s	C_α	C_β	O	O_H	H_O
$(OOH)^q$	**0**	**2**	**–**	**–**	**0.742**	**0.268**	**–0.010**
	–1	1	–	–	0.000	0.000	0.000
	–1	3	–	–	1.479	0.535	–0.014
Ph—CH=CH_2	**0**	**1**	**0.000**	**0.000**	**0.000**	**0.000**	**0.000**
Reaction path A							
$[CuL(OOH)]^q$	0	1	–	–	0.701	0.310	–0.008
	0	3	–	–	0.702	0.309	–0.008
	–1	**2**	**–**	**–**	**0.097**	**0.007**	**0.001**
$\{[CuL(OH)](Ph—CH_2—CHO)\}^q$	0	1	–0.002	–0.004	–0.005	–0.343	0.008
	0	3	0.002	0.004	0.005	0.435	–0.011
	–1	**2**	**0.000**	**0.000**	**0.000**	**0.035**	**–0.001**
Reaction path B							
$[CuL(Ph—CH=CH_2)]^q$	**–1**	**1**	**0.000**	**0.000**	**–**	**–**	**–**
	–1	3	0.042	0.174	–	–	–
	0	2	0.000	0.000	–	–	–
$\{CuL[Ph—CH(OOH)—CH_2]\}^q$	0	1	0.035	–0.998	–0.021	–0.006	0.000
	0	3	–0.029	0.982	0.065	0.000	0.000
	–1	**2**	**–0.001**	**0.254**	**0.022**	**–0.001**	**0.000**
Reaction path B							
$[CuL]^q$	0	2	0.526	0.115(2×)		0.111(2×)	0.006(2×)
	–1	**1**	**0.000**	**0.000(2×)**		**0.000(2×)**	**0.000(2×)**
	–1	3	0.590	0.090		0.098	0.001
				0.345		0.115	0.006
$[CuL(OOH)]^q$	0	1	–0.532	–0.110(2×)		–0.111	–0.011
						–0.116	–0.006
	0	3	0.525	0.110(2×)		0.110	0.011
						0.116	0.006
	–1	2	0.575	0.054		0.106(2×)	0.002
				0.047			0.004
$\{[CuL(OH)](Ph—CH_2—CHO)\}^q$	0	1	0.197	0.104(2×)		–0.061	0.008
						0.022	0.003
	0	3	0.673	0.138(2×)		0.296	0.050
						0.186	0.008
	–1	**2**	**0.610**	**0.059**		**0.109**	**0.000**
				0.065		**0.106**	**0.002**
Reaction path C							
$[CuL(Ph—CH=CH_2)]^q$	–1	1	0.000	0.000		0.000	0.000
	–1	3	0.571	0.153		0.111	0.000
				0.166		0.108	0.002
	0	2	0.526	0.115(2×)		0.112	0.006(2×)
						0.110	
$\{CuL[Ph—CH(OOH)—CH_2]\}^q$	0	1	0.527	0.115(2×)		0.112	0.007(2×)
						0.109	
	0	3	0.527	0.115(2×)		0.111(2×)	0.007(2×)
	–1	2	0.507	0.000		0.083	–0.001
				0.023		0.087	0.002

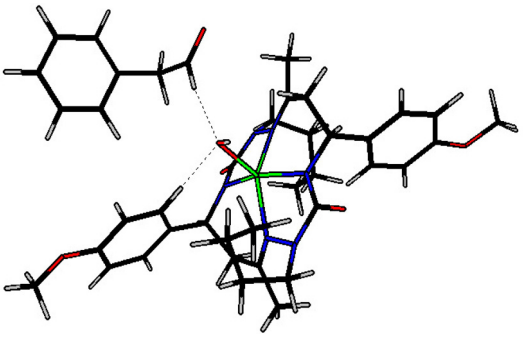

Fig. 4. DFT optimized structure of $\{[CuL(O_H—H_O)](Ph—C_\alpha H_2—C_\beta HO)\}^-$ in doublet spin state (Cu – green, C – black, N – blue, O – red, H – gray).

Reaction pathway B

Structures of $[CuL(Ph—CH=CH_2)]^q$ were optimized starting from $[CuL]^q$ with added neutral styrene in form of a π-complex with Cu—$C_{\alpha/\beta}$ distances of ca 2.4 Å. Only the optimized structure of $^1[CuL(Ph—CH=CH_2)]^-$ preserved the original form of a π-complex where the Cu—$C_{\alpha/\beta}$ bond lengths are comparable with the Cu—N1/N3 ones and the square-planar Cu coordination lost its planarity (Fig. 5, Tabs. A2–A3 in Appendix). Its $^2[CuL(Ph—CH=CH_2)]^0$ and $^3[CuL(Ph—CH=CH_2)]^-$ analogues with separated square-planar $[CuL]^q$ and neutral Ph—CH=CH_2 components are energetically higher (Tabs. 1 and A1–A3, and Fig. A4 in Appendix).

The lower charge and absence of spin at Cu in $^1[CuL(Ph—CH=CH_2)]^-$ indicates the formal oxidation state of Cu(I) unlike the Cu(II) one in $[CuL]^q$, $^2[CuL(Ph—CH=CH_2)]^0$, and $^3[CuL(Ph—CH=CH_2)]^-$ (Tabs. 2–3). The Cu—N1/N3 bonds in $^1[CuL(Ph—CH=CH_2)]^-$ are weaker than in $[CuL]^q$ and they are comparable with the Cu—$C_{\alpha/\beta}$ ones (Tab. 4). The C_α=C_β bond strength is equal to that of free styrene (Tab. 4).

According to our results, the only stable π-complex can be obtained by the non-radical endothermic reaction

$$^1[CuL]^- + Ph—CH=CH_2 \rightarrow \rightarrow {}^1[CuL(Ph—CH=CH_2)]^- \quad (11)$$

as indicated by the reaction Gibbs energy, Δ_rG_{298} = +91.95 kJ/mol under normal conditions (Tab. A1 in Appendix).

An addition of the hydroperoxyl radical to $^1[CuL(Ph—CH=CH_2)]^-$ leads to $^2\{CuL[Ph—CH(OOH)—CH_2]\}^-$ with a split Cu—C_α bond and hydroperoxyl bonding to the C_α site (Fig. 6, Tabs. A2–A3 in Appendix). Subsequently, the spin density is shifted from hydroperoxyl to Cu with a higher positive charge corresponding to the real oxidation state instead of Cu(I) in $^1[CuL(Ph—CH=CH_2)]^-$ (Tabs. 2 and 3). The Cu—N1/N3 bonds are weaker than the Cu—C_β one in $^1[CuL(Ph—CH=CH_2)]^-$ (Tab. 4).

Electron removal from $^1[CuL(Ph—CH=CH_2)]^-$ should correspond to the formal oxidation state Cu(II) but it causes the Ph—CH(OOH)—CH_2 split from the $[CuL]^0$ unit (Tabs. A2–A3 and Fig. A5 in Appendix) with higher energies (Tabs. 1 and A1 in Appendix). Based on charges and spin populations (Tabs. 2 and 3), real Cu(II) oxidation state is preserved in neutral $[CuL(Ph—CH=CH_2)]^0$ complexes and the spin density is shifted from hydroperoxyl to N1 and N3 atoms.

Our results show that the most advantageous hydroperoxyl addition to the above mentioned π-complex can be described by the following endothermic reaction

$$^1[CuL(Ph\text{-}CH=CH_2)]^- + {}^2(OOH)^0 \rightarrow \rightarrow {}^2\{CuL[Ph\text{-}CH(OOH)\text{-}CH_2]\}^- \quad (12)$$

as indicated by the reaction Gibbs energy, Δ_rG_{298} = 35.92 kJ/mol under normal conditions (Tab. A1 in Appendix).

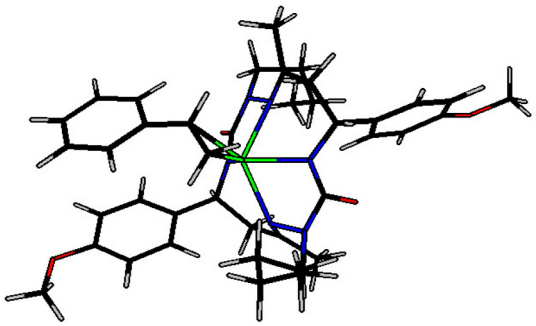

Fig. 5. DFT optimized structure of $[CuL(Ph—C_\alpha H=C_\beta H_2)]^-$ in singlet spin state (Cu – green, C – black, N – blue, O – red, H – gray).

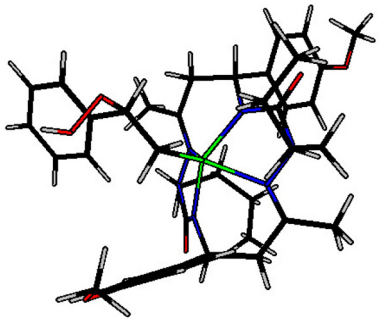

Fig. 6. DFT optimized structure of $\{CuL[Ph—C_\alpha H(O—O_H—H_O)—C_\beta H_2]\}^-$ in doublet spin state (Cu – green, C – black, N – blue, O – red, H – gray).

Tab. 4. Overlap weighted bond orders between C_α, C_β, O, O_H, and H_O atoms in (O—O_H—H_O) and (Ph—C_αH═$C_\beta H_2$) units, and Cu and N atoms in the complexes under study with charges q and spin multiplicities M_s. Data related to systems included in reaction pathways A and B are in bold.

	q	M_s	C_α—C_β	C_α—O	C_α—O_H	C_β—O	C_β—O_H	O—O_H
$(OOH)^q$	**0**	**2**	**–**	**–**	**–**	**–**	**–**	**0.679**
	–1	1	–	–	–	–	–	0.417
	–1	3	–	–	–	–	–	0.090
Ph—CH═CH_2	**0**	**1**	**1.380**	**–**	**–**	**–**	**–**	**–**
Reaction path A								
$[CuL(OOH)]^q$	0	1	–	–	–	–	–	0.720
	0	3	–	–	–	–	–	0.719
	–1	**2**	**–**	**–**	**–**	**–**		**0.505**
$\{[CuL(OH)](Ph—CH_2—CHO)\}^q$	0	1	0.868	–0.027	0.000	1.292	–0.012	0.001
	0	3	0.869	–0.026	0.000	1.294	–0.007	0.001
	–1	**2**	**0.855**	**–0.027**	**0.001**	**1.282**	**–0.017**	**0.001**
Reaction path B								
$[CuL(Ph—CH═CH_2)]^q$	**–1**	**1**	**1.279**	**–**	**–**	**–**	**–**	**–**
	–1	3	1.279	–	–	–	–	–
	0	2	1.379	–	–	–	–	–
$\{CuL[Ph—CH(OOH)—CH_2]\}^q$	0	1	0.949	0.722	–0.025	–0.025	0.000	0.530
	0	3	0.958	0.690	–0.024	–0.019	–0.001	0.529
	–1	**2**	**0.975**	**0.668**	**–0.027**	**–0.043**	**–0.005**	**0.524**
Reaction path A								
$[CuL]^q$	0	2	0.260(2×)		0.339(2×)		–	–
	–1	**1**	**0.188(2×)**		**0.298(2×)**		**–**	**–**
	–1	3	0.272		0.338		–	–
			0.357		0.346			
$[CuL(OOH)]^q$	0	1	0.232		0.311		0.069	–
			0.230		0.305		0.015	
	0	3	0.232		0.310		0.070	–
			0.230		0.305		0.015	
	–1	**2**	**0.238**		**0.305**		**0.302**	**–**
			0.215		**0.313**		**0.023**	
$\{[CuL(OH)](Ph—CH_2—CHO)\}^q$	0	1	0.293		0.384		0.000	0.000(2×)
			0.297		0.391		0.333	
	0	3	0.287		0.362		0.000	0.000(2×)
			0.295		0.386		0.333	
	–1	**2**	**0.241**		**0.308**		**–0.001**	**0.004**
			0.233		**0.310**		**0.309**	**0.009**
Reaction path B								
$[CuL(Ph—CH═CH_2)]^q$	**–1**	**1**	**0.172**		**0.220**		**–**	**0.195**
			0.132		**0.240**			**0.240**
	–1	3	0.287		0.332(2×)		–	–0.001
			0.294					0.007
	0	2	0.259(2×)		0.338(2×)		–	0.001(2×)
$\{CuL[Ph—CH(OOH)—CH_2]\}^q$	0	1	0.258(2×)		0.337		0.000(2×)	0.000(2×)
					0.333			
	0	3	0.258		0.337		0.000(2×)	0.000(2×)
			0.260		0.339			
	–1	**2**	**0.161**		**0.277**		**0.010**	**0.052**
			0.178		**0.262**		**0.003**	**0.324**

Discussion

Using quantum-chemical treatment, relevant intermediates in various charge and spin states were investigated for three reaction pathways of styrene oxidation by hydroperoxyl. The alternative reaction pathways A and B are based on the $[CuL]^q$ catalyst (Fig. 1), most probably its anionic form in the singlet spin state corresponding to the formal oxidation state of Cu(I). In the reaction pathway A, the neutral hydroperoxyl radical is bonded to Cu to form $^2[CuL(OOH)]^-$ (Fig. 3), which is unstable in other charge and spin states. Spin density is shifted to Cu, which corresponds to the real oxidation state of Cu(II). Subsequent addition of neutral styrene results in $^2\{[CuL(OH)](Ph—CH_2—CHO)\}^-$ formation after significant O and H atoms rearrangement; here, only weakly bonded $^2[CuL(OH)]^-$ and $Ph—CH_2—CH═O$ units are present. This reaction pathway seems to be realistic, but the Cu—OH split must be solved (probably by reaction with hydroperoxyl as in Lashanizadegan et al. (2017; 2021)) as well as the formation of benzaldehyde (by interaction with hydroperoxyl (Lashanizadegan et al., 2021) or with $^2[CuL(OH)]^-$ (Zhou et al., 2010; Yang and Sarazen, 2022).

Reaction pathway B starts with the initial non-radical formation of the π-complex $^1[CuL(Ph—CH═CH_2)]^-$ (Fig. 5) in Cu(I) oxidation state (Eq. 11); this reaction is problematic because of its endothermic character. However, its analogues in other charge and spin states do not allow for such π-complex formation. Subsequent addition of a hydroperoxyl radical leads to $^2\{CuL[Ph—CH(OOH)—CH_2]\}^-$ (Fig. 6) with $Cu—C_\beta$ bonding. Its oxidation leads to $Ph—CH(OOH)—CH_2$ separation.

Conclusions

Our DFT study compared two possible reaction pathways of styrene oxidation by hydrogen peroxide under CuL catalysis, where H_2L = *trans*-2,9-dibutyl-7,14-dimethyl-5,12-di(4-methoxyphenyl)-1,2,4,8,9,11-hexaazacyclotetradeca-7,14-diene-3,10-dione. Despite the restriction to the main reaction intermediates, our results indicate that the reaction starts more probably by the formation of $^2[CuL(OOH)]^-$ (reaction pathway A). The alternative reaction pathway B starting with $^1[CuL(Ph—CH═CH_2)]^-$ is afflicted by the endothermic character of this π-complex formation. Possible charge and spin states of the relevant reaction intermediates were also identified. Results of quantum-chemical calculations in vacuum indicate that the exothermic reaction path A (Δ_rG_{298} = –323.04 kJ/mol), which contains two exothermic reaction steps (see Eqs. (9) and (10)), is preferred over the endothermic reaction path B (Δ_rG_{298} = 127.87 kJ/mol), which contains two endothermic reaction steps (see Eqs. (11) and (12)). Future studies should provide additional details on the realistic reaction mechanism, including solvent effects.

Acknowledgement

Slovak Grant Agency VEGA (contract No. 1/0175/23) is acknowledged for financial support. The author thanks the HPC center at the Slovak University of Technology in Bratislava, which is a part of the Slovak Infrastructure of High-Performance Computing (SIVVP project ITMS 26230120002, funded by European Region Development Funds) for the computational time and resources made available.

References

Abuhafez N, Ehlers AW, de Bruin B, Gramage-Doria R (2024) Angew. Chem. Int. Ed. 63: e202316825.

Andrade MA, Martins LMDRS (2021) Molecules 26: 1680 and the references cited in.

Becke AD (1993) J. Chem. Phys. 98: 5648—5652.

Carpenter JE, Weinhold F (1988) J. Mol. Struct. (THEOCHEM) 169: 41—62.

Dobrov A, Fesenko A, Yankov A, Stepanenko I, Darvasiova D, Breza M, Rapta P, Martins LMDRS, Pombeiro AJL, Shutalev A, Arion VB (2020) Inorg. Chem. 59: 10650—10664.

Foster JP, Weinhold, F (1980) J. Am. Chem. Soc. 102: 7211—7218.

Frisch MJ, Trucks GW, Schlegel HB, Scuseria GE, Robb MA, Cheeseman JR, Scalmani G, Barone V, Petersson GA, Nakatsuji H, Li X, Caricato M, Marenich AV, Bloino J, Janesko BG, Gomperts R, Mennucci B, Hratchian HP, Ortiz JV, Izmaylov AF, Sonnenberg JL, Williams-Young D, Ding F, Lipparini F, Egidi F, Goings J, Peng B, Petrone A, Henderson T, Ranasinghe D, Zakrzewski VG, Gao J, Rega N, Zheng G, Liang W, Hada M, Ehara M, Toyota K, Fukuda R, Hasegawa J, Ishida M, Nakajima T, Honda Y, Kitao O, Nakai H, Vreven T, Throssell K, Montgomery JA Jr, Peralta JE, Ogliaro F, Bearpark MJ, Heyd JJ, Brothers EN, Kudin KN, Staroverov VN, Keith TA, Kobayashi R, Normand J, Raghavachari K, Rendell AP, Burant JC, Iyengar SS, Tomasi J, Cossi M, Millam JM, Klene M, Adamo C, Cammi R, Ochterski JW, Martin RL, Morokuma K, Farkas O, Foresman JB, Fox DJ (2016) Gaussian 16, Rev C01, Gaussian, Inc., Wallingford, CT.

Keith JA, Henry PM (2009) Angew. Chem. Int. Ed. 48: 9038—9049.

Lashanizadegan M, Alavijeh RK, Anafcheh M (2017) J. Mol. Struct. 1146: 450—457.

Lashanizadegan M, Ashari HA, Sarkheil M, Anafcheh M, Jahangiry S (2021) Polyhedron 200: 115148.

Lashanizadegan M, Habibi N, Mirzazadeh H, Ghiasi M (2022) React. Kinet., Mechan. Catal. 135: 3223—3242.

Malrieu J-P, Trinquier G (2012) J. Phys. Chem. A 116: 8226—8237.

Razmara Z, Necas M, Karimi P (2025) J. Mol. Struct. 1330: 141440.
Reed AE, Curtiss LA, Weinhold F (1988) Chem. Rev. 88: 899–926.
Sayeh K, Louroubi A, Abdallah N, Fkhar L, Aflak N, Bahsis L, Hasnaoui A, Ali MA, El Firdoussi L (2025) React. Kinet., Mechan. Catal. 138: 911–927.
Ugliengo P (2012) MOLDRAW: A Program to Display and Manipulate Molecular and Crystal Structures, University Torino, Torino. Available online: https://moldraw.software.informer.com (accessed on 9 September 2019).
Vala G, Jadeja RN, Patel A, Choquesillo-Lazarte D (2024) Inorg. Chim. Acta 563: 121925.
Wu Y, Kang J, Gao W, Bi M, Yang D, Ji R, Meng Q, Ma C (2023) J. Comput. Chem. 44: 1917–1927.
Yang RA, Sarazen ML (2022) ACS Catal. 12: 14476–14491.
Zhou Sh, Chen X, Qia Ch (2010) Chem. Phys. Let. 488: 44–49.

Appendix

Tab. A1. DFT energies, E_{DFT}, and Gibbs energies at 298 K, G_{298}, of compounds under study with charges q, spin multiplicities M_s, and spin squares $<S^2>$. Most stable systems are in bold.

	q	M_s	$<S^2>$	E_{DFT} [hartree]	G_{298} [hartree]
H_2L	0	1	0.000	–1876.93425	–1876.26433
Ph—CH═CH_2	0	1	0.000	–309.71674	–309.61529
$(OOH)^q$	0	2	0.754	–150.95195	–150.96003
	–1	1	0.000	**–150.98813**	**–150.99705**
	–1	3	2.014	–150.96260	–150.97652
Reaction path A:					
$[CuL]^q$	0	2	0.754	–3516.26778	–3515.61885
	–1	1	0.000	**–3516.31625**	**–3515.67541**
	–1	3	2.007	–3516.28161	–3515.63809
	+1	1	0.000	–3516.03126	–3515.37966
	+1	3	2.011	–3516.01984	–3515.37085
$[CuL(OOH)]^q$	0	1	1.008	–3667.23105	–3666.56946
				–3667.23104[a)]	–3666.56843[a)]
	0	3	2.008	–3667.23106	–3666.57048
	–1	2	0.754	**–3667.31654**	**–3666.65691**
$\{[CuL(OH)](Ph—CH_2—CHO)\}^q$	0	1	0.554	–3977.02647	–3976.24456
				–3977.02660[a)]	–3976.24371[a)]
	0	3	2.011	–3977.02613	–3976.24679
	–1	2	0.753	**–3977.14931**	**–3976.37377**
Reaction path B:					
$[CuL(Ph—CH═CH_2)]^q$	–1	1	0.000	**–3826.02113**	**–3825.25568**
	–1	3	2.006	–3826.00673	–3825.24806
	0	2	0.754	–3825.98858	–3825.22719
$\{CuL[Ph—CH(OOH)—CH_2]\}^q$	0	1	1.008	–3976.93793	–3976.15870
				–3976.94032[a)]	–3976.15974[a)]
	0	3	2.008	–3976.93556	–3976.15767
	–1	2	0.754	**–3977.01077**	**–3976.22939**

[a)]Corrected according to Eq. (8)

Tab. A2. Selected bond lengths (in Å) between relevant atoms in compounds under study with charges q and spin multiplicities M_s (see Fig. 1 and Tab. 2 for atom notation). Data related to systems included in reaction pathways A and B are in bold.

	q	M_s	C_α—C_β	C_α—O	C_α—O_H	C_β—O	C_β—O_H	O—O_H	N3 · · · H_O
$(OOH)^q$	0	2	–	–	–	–	–	1.326	–
	–1	**1**	**–**	**–**	**–**	**–**	**–**	**1.519**	**–**
	–1	3	–	–	–	–	–	2.222	–
Ph—CH=CH_2	0	1	1.337	–	–	–	–	–	–
Reaction path A									
$[CuL(OOH)]^q$	0	1	–	–	–	–	–	1.326	1.795
	0	3	–	–	–	–	–	1.326	1.794
	–1	**2**	**–**	**–**	**–**	**–**	**–**	**1.473**	**2.298**
$\{[CuL(OH)](Ph—CH_2—CHO)\}^q$	0	1	1.519	2.411	4.376	1.212	3.236	3.750	5.123
	0	3	1.519	2.412	4.418	1.211	3.271	3.770	2.568
	–1	**2**	**1.527**	**2.406**	**3.943**	**1.216**	**3.127**	**3.944**	**2.998**
Reaction path B									
$[CuL(Ph—CH=CH_2)]^q$	**–1**	**1**	**1.373**	**–**	**–**	**–**	**–**	**–**	**–**
	–1	3	1.359	–	–	–	–	–	–
	0	2	1.338	–	–	–	–	–	–
$\{CuL[Ph—CH(OOH)—CH_2]\}^q$	0	1	1.486	1.457	2.375	2.435	2.849	1.449	8.104
	0	3	1.484	1.474	2.384	2.443	2.884	1.447	8.733
	–1	**2**	**1.496**	**1.491**	**2.410**	**2.513**	**2.985**	**1.450**	**6.490**

Tab. A2. (cont.)

	q	M_s	Cu—N1	Cu—N3	Cu—O/O_H	Cu—$C_{\alpha/\beta}$
Reaction path A						
[CuL] (exp.)	0	–	1.962(2) (2×)	1.867(2) (2×)	–	–
$[CuL]^q$	0	2	2.002(2×)	1.892(2×)	–	–
	–1	**1**	**2.135(2×)**	**1.905(2×)**	**–**	**–**
	–1	3	2.021	1.921	–	–
			1.934	1.908		
$[CuL(OOH)]^q$	0	1	2.018	1.912	3.285	–
			2.016	1.886	3.506	
	0	3	2.017(2×)	1.913	3.277	–
				1.886	3.503	
	–1	**2**	**2.095**	**1.948**	**2.049**	**–**
			2.140	**1.941**	**2.914**	
$\{[CuL(OH)](Ph—CH_2—CHO)\}^q$	0	1	2.046	1.872	5.064	5.881
			2.023	1.885	2.039	4.755
	0	3	2.051	1.928	4.946	5.745
			2.031	1.907	1.992	4.633
	–1	**2**	**2.106**	**1.957**	**5.118**	**4.964**
			2.090	**1.961**	**2.064**	**4.398**
Reaction path B						
$[CuL(Ph—CH═CH_2)]^q$	**–1**	**1**	**2.282**	**2.164**	**–**	**2.212**
			2.448	**2.035**		**2.114**
	–1	3	1.980	1.905	–	6.715
			1.969	1.908		6.200
	0	2	2.002	1.891		6.513
			2.001	1.893		7.013
$\{CuL[Ph—CH(OOH)—CH_2]\}^q$	0	1	2.000	1.891	8.398	8.642
			2.001	1.894	7.060	8.561
	0	3	2.006	1.891(2×)	7.748	6.808
			2.003		7.253	5.843
	–1	**2**	**2.106**	**1.957**	**5.118**	**4.964**
			2.090	**1.961**	**2.064**	**4.398**

Tab. A3. Selected bond angles (in degrees) in compounds under study with charges q and spin multiplicities M_s (see Fig. 1 and Table 2 for atom notation). Data related to systems included in reaction pathways A and B are in bold.

	q	M_s	N1—Cu—N1'	N3—Cu—N3'	N1—Cu—N3	N3—Cu—N1' N1—Cu—N3'
Reaction path A						
$[CuL]^q$ (exp.)			180.0	180.0	82.83(7) (2×)	97.17(7) (2×)
$[CuL]^q$	0	2	180.0	180.0	82.2(2×)	97.8(2×)
	–1	**1**	**180.0**	**180.0**	**81.4(2×)**	**98.6(2×)**
	–1	3	176.8	177.0	81.3	95.8
					83.2	99.7
$[CuL(OOH)]^q$	0	1	169.3	177.0	82.7	97.3
					82.4	98.2
	0	3	169.3	177.0	82.8	98.1
					82.3	97.3
	–1	**2**	**139.7**	**159.4**	**79.4**	**94.5**
					79.1	**92.7**
$\{[CuL(OH)](Ph—CH_2—CHO)\}^q$	0	1	156.1	165.7	81.2	95.6
					95.7	95.7
	0	3	158.9	158.6	79.8	95.7
					81.5	95.1
	–1	**2**	**142.1**	**155.6**	**78.3**	**92.8**
					79.6	**93.4**
Reaction path B						
$[CuL(Ph—CH=CH_2)]^q$	**–1**	**1**	**124.9**	**123.7**	**70.8**	**79.6**
					71.0	**88.2**
	–1	3	179.9	179.6	82.4(2×)	97.7
						97.5
	0	2	179.4	179.9	82.2(2×)	97.7(2×)
$\{CuL[Ph—CH(OOH)—CH_2]\}^q$	0	1	179.5	179.9	82.3	97.8(2×)
					82.1	
	0	3	178.3	179.8	82.3(2×)	97.5
						97.9
	–1	**2**	**142.1**	**155.6**	**78.3**	**92.8**
					79.6	**93.4**

Tab. A3. (cont.)

	q	M_s	N1—Cu—O	N3—Cu—O	N1—Cu—$C_{\alpha/\beta}$	N3—Cu—$C_{\alpha/\beta}$
Reaction path A						
$[CuL]^q$ (exp.)			–	–	–	–
$[CuL]^q$	0	2	–	–	–	–
	–1	**1**	**–**	**–**	**–**	**–**
	–1	3	–	–	–	–
$[CuL(OOH)]^q$	0	1	106.0	74.2	–	–
			95.4	52.8		
	0	3	106.1	74.4	–	–
			95.6	52.8		
	–1	**2**	**128.3**	**96.4**	**–**	**–**
			105.3	**79.0**		
$\{[CuL(OH)](Ph—CH_2—CHO)\}^q$	0	1	145.9	93.0	133.1	113.6
			105.8	90.6	137.2	102.9
	0	3	145.2	96.0	132.3	117.6
			101.5	90.4	101.5	106.4
	–1	**2**	**162.7**	**104.3**	**145.2**	**131.8**
			117.6	**100.7**	**154.1**	**114.7**
Reaction path B						
$[CuL(Ph—CH═CH_2)]^q$	**–1**	**1**	**–**	**–**	**143.0**	**119.3**
					110.7	**96.7**
	–1	3	–	–	118.9	49.9
					110.9	51.8
	0	2	–	–	116.3	144.6
					111.2	137.5
$\{CuL[Ph—CH(OOH)—CH_2]\}^q$	0	1	101.1	134.1	109.1	138.8
			100.1	130.1	117.6	131.9
	0	3	107.3	110.5	115.0	106.1
			99.9	117.5	108.6	97.7
	–1	**2**	**162.7**	**104.3**	**145.2**	**131.8**
			117.6	**100.7**	**117.6**	**114.7**

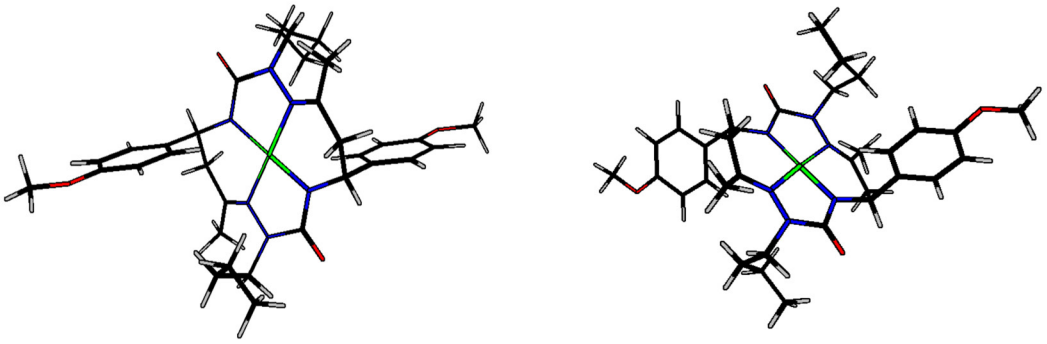

q = 0 M_s = 2 q = –1 M_s = 3

Fig. A1. DFT optimized structure of $[CuL]^q$ in various spin states (Cu — green, C — black, N — blue, O — red, H — gray).

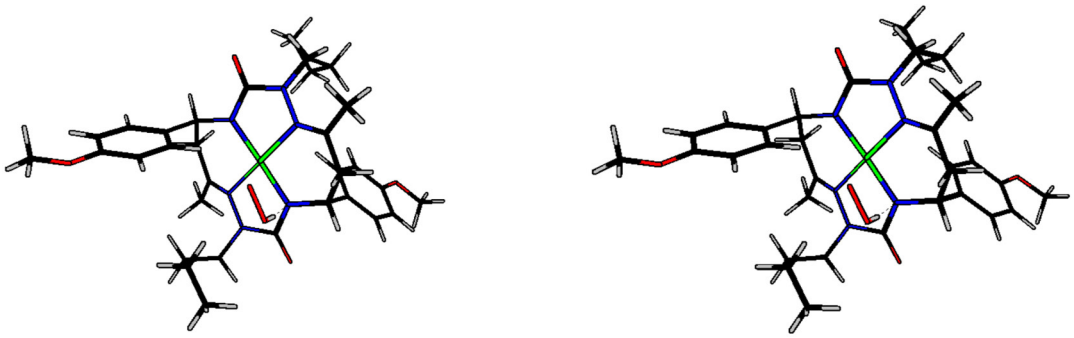

q = 0 M_s = 1 q = 0 M_s = 3

Fig. A2. DFT optimized structure of $[CuL(O—O_H—H_O)]^0$ in singlet and triplet spin states (Cu — green, C — black, N — blue, O — red, H — gray).

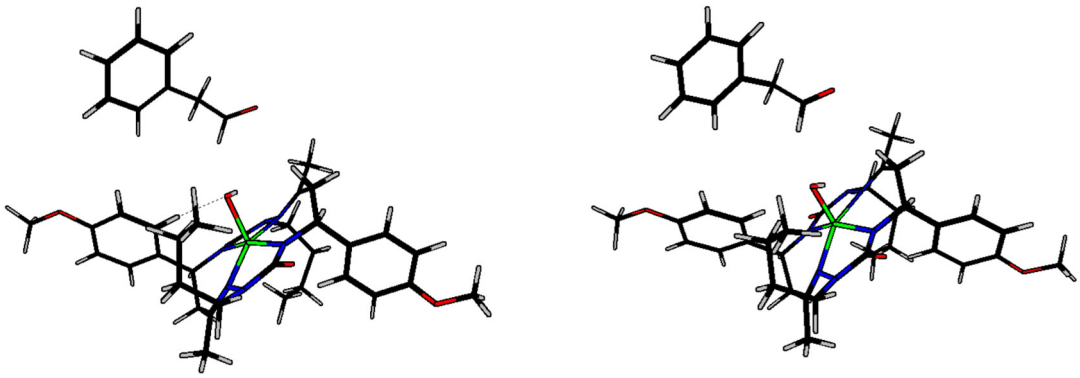

q = 0 M_s = 1 q = 0 M_s = 3

Fig. A3. DFT optimized structure of $\{[CuL(O_H—H_O)](Ph—C_\alpha H_2—C_\beta HO)\}^0$ in singlet and triplet spin states (Cu — green, C — black, N — blue, O — red, H — gray).

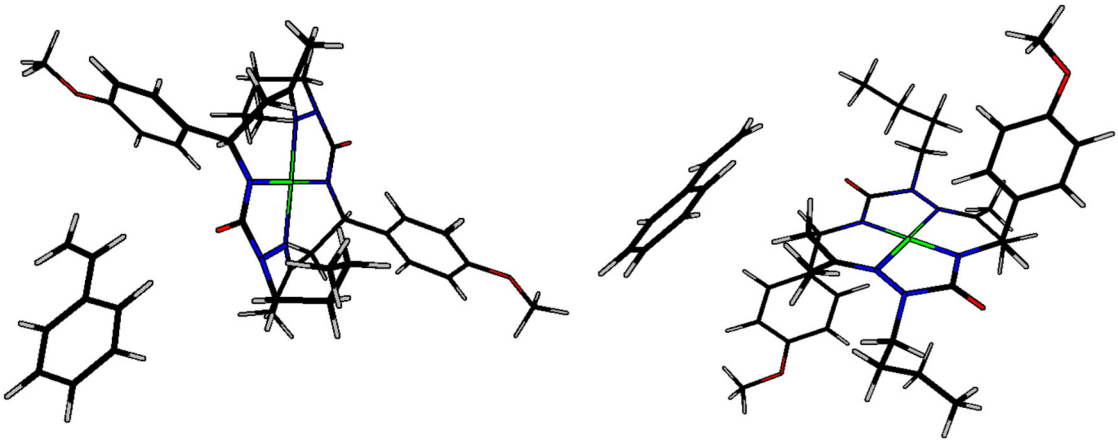

q = 0 M_s = 2 q = –1 M_s = 3

Fig. A4. DFT optimized structure of $[CuL(Ph—C_{\alpha}H═C_{\beta}H_2)]^q$ in various spin states (Cu – green, C – black, N – blue, O – red, H – gray).

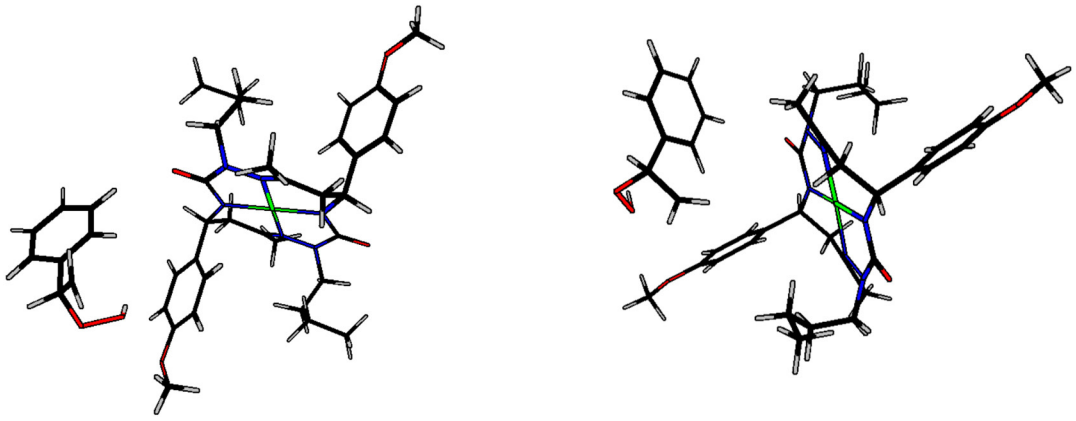

q = 0 M_s = 1 q = 0 M_s = 3

Fig. A5. DFT optimized structure of $\{CuL[Ph—C_{\alpha}H(O—O_H—H_O)—C_{\beta}H_2]\}^0$ in singlet and triplet spin states (Cu –green, C – black, N – blue, O – red, H – gray).